https://doi.org/10.5194/ar-2026-21
Preprint. Discussion started: 2 June 2026

AEROSOL Research Discussions

The influence of hydrogen addition on carbonaceous aerosols produced by an ethylene flame

Stijn S.A. van Rijn[1], Haiyan Ni[2], Martijn A.R. Goudberg[1], Merel R. van Helten[1], Anatoli Mokhov[1], Ulrike Dusek[1]

[1]ESRIG, University of Groningen, Nijenborh 6, 9747 AG, Groningen, The Netherlands
[2]School of Environmental and Municipal Engineering, Xi'An University of Architechture and Technology, Xi'An, 710055, China

Correspondence to: Ulrike Dusek (u.dusek@rug.nl)

Abstract. Combusting hydrogen alongside carbon-based fuels has been proposed to reduce CO_2 emissions and combat climate change. However, combustion-generated aerosol particles can also cause a significant radiative forcing on climate. Since addition of novel fuels alters the combustion process, it also influences particle formation inside the fame and consequently the properties of the emitted aerosols. To investigate this, combustion-generated particles from various ethylene/hydrogen mixtures are sampled in the post-flame regime. The size distribution and light absorption properties of the particles are measured using a scanning mobility particle sizer (SMPS) and a multi-wavelength aethalometer. In addition, the particles are sampled on quartz-fiber filters and the mass concentrations of organic, elemental and total carbon (OC, EC, and TC) are measured using a thermo-optical OC-EC analyzer. The geometric mean diameter of the emitted particles decreased from 300 nm down to 150 nm upon increasing the hydrogen mole fraction in the fuel from 0% to 50%, while the EC/TC fraction decreased from 70% to 35%. The light absorption of methanol-dissolved OC were measured using UV-vis analysis, showing no dependence on flame parameters or fuel composition, and no significant light absorption at wavelengths larger than 500 nm. For combustion-generated particles, the mass absorption cross section σ of the total carbonaceous aerosol (i.e. the absorption coefficient normalized to TC mass concentration) is reported as a function of EC/TC ratio at wavelengths of 370, 590 and 880 nm. At a wavelength of 880 nm, σ is slightly higher than expected of an external mixture of OC and EC, indicating some absorption enhancement due to OC coating. At wavelengths of 590 and 370 nm, σ is much higher than that expected for a mixture of colorless OC and EC and this enhancement is attributed to light absorbing non-refractory species, also called brown carbon (BrC). The absorption Ångström exponent (370 - 660 nm) increased from 1.3 up to 3.8 with increasing hydrogen mole fraction in the fuel, especially at lower flame temperatures, indicating an increasing contribution of BrC to the light absorption of the emitted particles. It is concluded that BrC is a precursor to EC during particle formation, in line with the existing literature, and that it matures less efficiently into EC in the hydrogen containing flame.

https://doi.org/10.5194/ar-2026-21
Preprint. Discussion started: 2 June 2026

AEROSOL Research Discussions

1 Introduction

The urgent need to mitigate climate change is leading to a transition towards carbon-free or low-carbon fuels. Novel fuels such as hydrogen, methanol or ammonia offer promising alternatives to the current fossil fuels by lowering the carbon footprint (García et al., 2024; Gülder et al., 1996; Hui et al., 2023; Khanehzar et al., 2022; Liu et al., 2021; Montgomery et al., 2021; Ren et al., 2022; Wu et al., 2024; Yan et al., 2019). Mixing these novel fuels with conventional carbon-holding fuels can be regarded as a first step, as this approach could utilize the advantages of both fuel types. Co-combusting traditional and carbon-free fuels could facilitate a smooth transition from the current carbon-based energy infrastructure towards a more sustainable future, while maintaining the current energy output.

Carbonaceous aerosols emitted by combusting fossil fuels can have a significant warming effect on the climate (IPCC, 2023). Their radiative forcing depends on their optical properties, which are determined by e.g., particle size, shape, mixing state and chemical composition, in particular the relative contribution of organic carbon (OC) and elemental carbon (EC) to the total carbon content of the particle (Myhre et al., 2013). It is therefore crucial to understand how particle properties change, when novel fuels are mixed with conventional fuels. Classification of carbonaceous aerosol according to optical properties usually distinguishes black carbon (BC), colored carbon (also referred to as brown carbon, BrC) and colorless OC (Pöschl, 2005). The term BC is sometimes used as synonymous to EC, however the latter term is defined according to thermo-chemical properties instead of optical properties. BC has an imaginary refractive index independent of wavelength, and therefore it strongly warms the climate through efficient light absorption in a broad range of wavelengths (Bond et al., 2013; Bond and Bergstrom, 2006). BrC is classified as carbonaceous material that absorbs light in near-UV and some visible wavelengths, but not in the infrared region (Andreae and Gelencser, 2006). Due to its diversity, BrC can be further divided into subclasses based on specific optical properties (Saleh, 2020; Saleh et al., 2018). While BrC may also contribute to global warming, its overall effect remains uncertain (Kumar et al., 2018; Saleh, 2020). However, OC as a whole (including BrC) exerts a net cooling effect through scattering of sunlight and aerosol–cloud interactions (IPCC, 2023; Myhre et al., 2013).

EC and BrC contained in primary combustion emissions are produced inside flames, where carbonaceous radicals drive the formation and growth of polycyclic aromatic hydrocarbons (PAHs), which subsequently nucleate into particulate matter of complex and amorphous character (Jin et al., 2021; Xi et al., 2021). In the high-temperature region of the flame, the C/H ratio of these nascent particles increases as a result of de-hydrogenation, creating the turbostatic graphitic layers associated with BC particles. With increasing residence time in the flame, these primary particles agglomerate to fractal-shaped bigger particles. These matured particles exit the flame as a complex mixture of particulates consisting of both OC and EC. The emitted OC can be attributed to remaining precursors to EC (Malmborg et al., 2017; Maricq, 2014; Saleh et al., 2018; Török et al., 2018), for example not fully matured particles that escaped the flame before undergoing the complete de-hydrogenation. Their higher hydrogen content and less graphitic structure increase the likelihood that they are therefore classified as OC by e.g. thermal-optical analysis. Next to immature particulates, emitted VOCs such as PAH can condense on the particles in the cooler regions on the flame or in the post-flame regime, creating a coating on the particle. Condensed organic gases decrease the EC/TC ratio

https://doi.org/10.5194/ar-2026-21
Preprint. Discussion started: 2 June 2026

and contribute to the compaction of particles from a fractal to a more spherical morphology (Corbin et al., 2023). In the post-flame regime OC and EC can therefore be both internally and externally mixed, where external mixing refers to OC and EC as separate particles whereas the term internal mixing is used when one particle contains both compounds. Internal mixing can theoretically range from a homogeneous mixture of OC and EC to a so-called coated particle, where an EC core is coated with OC (Bond and Bergstrom, 2006; Lack and Langridge, 2013; Martins et al., 1998; Zhang et al., 2016). In combustion-generated particles, coated particles are a commonly observed phenomenon and the light absorption of the EC core can be increased by the coating, even if OC itself does not absorb any light, referred to as the lensing effect (Martins et al., 1998; Zhang et al., 2016; Zhao et al., 2021).

Various studies showed that aerosol properties of the combustion-generated particles depend upon flame temperature, fuel composition and equivalence (fuel to air) ratio. For example, a change towards smaller particle size distributions is reported when the propane fuel has been diluted by various amounts of nitrogen (Maricq, 2014). Furthermore, particles with decreasing EC/TC fractions and stronger relative near-UV light absorption are reported when increasing the equivalence ratio of toluene and benzene flames at various temperatures (Cheng et al., 2019). Therefore, it is crucial to know what effect co-combustion of novel fuels with conventional carbon-containing fuels will have on the properties of combustion-generated particles. This study will focus on hydrogen as a novel fuel.

Previous studies have shown that the total mass or number concentration of the emitted particles is reduced as a result of hydrogen addition to various ethylene flames (García et al., 2024; Gülder et al., 1996; Khanehzar et al., 2022; Wu et al., 2024). However, the change in particle properties upon adding hydrogen to ethylene flames has been less investigated. Therefore, the present study focuses on the properties of combustion-generated particles in hydrogen/ethylene mixtures, where ethylene is chosen for its particle formation potential, while hydrogen serves as a novel fuel. The change of physical and optical aerosol properties are investigated as a function of hydrogen fraction in the fuel and flame temperature. The generated particles are sampled on two different positions above the flame, creating an insight in the change in particle properties during the post-flame regime. Additionally, the relationship between optical properties and EC/TC of the generated particles is investigated.

https://doi.org/10.5194/ar-2026-21
Preprint. Discussion started: 2 June 2026

AEROSOL Research Discussions

2 Methods

2.1 Experimental setup

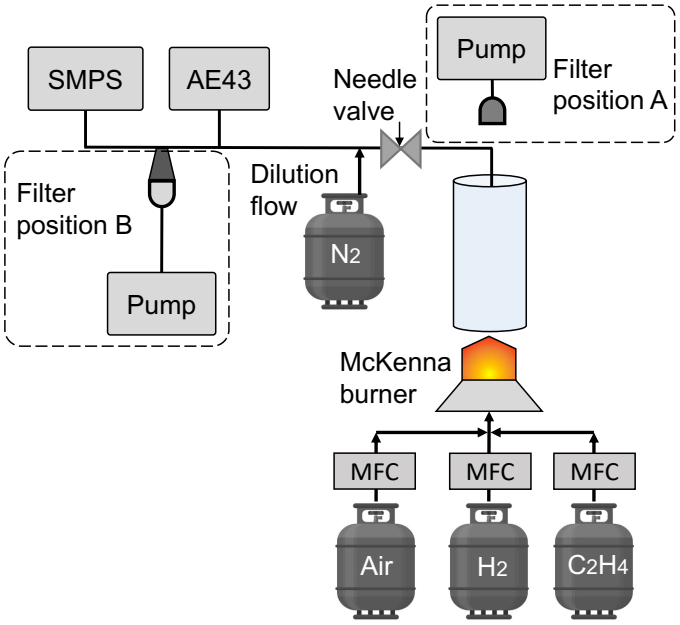

Figure 1: Schematic representation of experimental setup. A stable flow of gases is set using mass flow controllers (MFC), after which the gases mix and enter the McKenna burner. The combustion-generated particles are sampled and diluted in the aerosol inlet. AE43 aethalometer and SMPS are attached to the sample line. The dashed boxes represent the 2 different positions where the filter sampler was placed. In position A, the particles are sampled in the hot flue gases above the flame. In position B, the sample is first diluted and cooled down to room temperature before the particles are sampled.

The experimental setup is shown in Fig. 1. The premixed, flat, one-dimensional flames are produced using a water-cooled McKenna burner with a diameter of 60 mm (Senser et al., 1985). The air, hydrogen and ethylene flows are set individually by mass flow controllers (Bronkhorst Inc.) and subsequently mixed before entering the burner. After passing through the porous bronze plate, the homogeneous gas flow is ignited, forming a burner-stabilized one-dimensional flame. The position of the flame front relative to the burner head determines the flame temperature; at the closer positions heat losses are higher and thus the flame temperature is lower.

Under stationary conditions, the exit velocity, v_{exit}, should be equal to the propagation velocity of the flame front (burning velocity). Because the burning velocity depends upon the flame temperature (Warnatz et al., 2006), changing the exit velocity of the unburned gas mixture results in moving the flame front closer or farther from the burner head. The flame front will move to the position where the flame temperature balances the burning velocity equal to the exit velocity of the unburned gas mixture. Thus, varying the cold gas velocity results in varying flame temperatures at fixed equivalence ratio.

https://doi.org/10.5194/ar-2026-21
Preprint. Discussion started: 2 June 2026

AEROSOL Research Discussions

To prevent mixing with surrounding air and keeping a uniform equivalence (fuel to air) ratio φ, a shroud of nitrogen gas is formed around the porous plate, shielding the flame from the outside air. The overall reaction of combustion of hydrogen/ethylene/air mixture can be presented by the following expression:

$$\phi\big((1-\gamma)C_2H_4+\gamma H_2\big)+(3-2.5\gamma)(O_2+3.78N_2)\longrightarrow combustionproducts \quad (1)$$

where φ is the equivalence ratio (Warnatz et al., 2006) and γ is the mole fraction of hydrogen in the fuel. At φ > 1 combustion products can contain carbonaceous particles along with various gaseous species such as water, carbon oxides and hydrocarbons. The parameters γ and φ are determined from the measured mass flow rates of ethylene, hydrogen and air using the following relations

$$\gamma=\frac{f_{H_2}}{f_{H_2}+f_{C_2H_4}}, \quad (2)$$

$$\varphi=4.78(3-2.5\gamma)\frac{f_{H_2}+f_{C_2H_4}}{f_{air}}, \quad (3)$$

where f_{H2}, f_{C2H4} and f_{air} are volumetric flow rates of ethylene, hydrogen and air, respectively, expressed in standard liters per minute (SLPM). In the present work φ is kept constant at 2.3 while γ is varied in the range from 0 to 0.5. To vary the flame temperature while keeping the same fuel composition, the exit velocity of the cold gas mixture is varied between 6 cm s^{-1} and 10 cm s^{-1}.

Above the McKenna burner, a glass tube is placed to stabilize the exhaust flow while preventing mixing combustion products with surrounding air. In the upper region of the glass tube, an aerosol sampling inlet and a filter sampler are positioned at a height above the burner (HAB) of approximately 65 cm. The position of that filter sampler is called position A. The filter sampler can also be connected to the sample line in position B.

The sampling inlet is placed in the center at the top of the glass tube. The sampled flow of flue gases is then further diluted with nitrogen, with dilution factor around ~100. A Magee Scientific AE43 aethalometer, a Scanning Mobility Particle Sizer (SMPS) and a filter sampler can be connected to the sample line.

The AE43 is a dual-spot aethalometer and is used to measure the light attenuation of aerosol deposited on a filter strip at 7-wavelengths (370, 420, 520, 590, 660, 880 and 950 nm) with a time resolution of one minute. A nominal flow rate of 2 liters per minute was used. After some measurement time, the aethalometer needs to advance the tape to start with a fresh filter spot, at which point a new experiment was started. The filter loading effect is corrected by loading two filter spots at different flow rates (Drinovec et al., 2015).

The device accounts for multiple scattering using a constant factor, C_{scat}, which primarily depends on the filter material. However, recent studies (Ferrero et al., 2024; Kalbermatter et al., 2022; Kumar et al., 2018; Yus-Díez et al., 2021) have shown that the actual value of C_{scat} is often higher than the manual's default value of 1.39. Several values for C_{scat} are reported in the

https://doi.org/10.5194/ar-2026-21
Preprint. Discussion started: 2 June 2026

literature for a similar instrument (AE33), and the majority of the values are between 2 and 3, roughly double the manual's default value. This implies that using the default value might overestimate the true absorption coefficient.

Moreover, C_{scat} is not strictly constant, as it can vary with both wavelength and the scattering properties of the sampled aerosol (Ferrero et al., 2024; Yus-Díez et al., 2021). Higher values of C_{scat} are typically observed under atmospheric conditions for particles with a single scattering albedo > 0.9, whereas combustion-generated particles typically have a much lower single scattering albedo. Therefore, the wavelength dependence of C_{scat} is considered minimal for combustion aerosols (Corbin et al., 2018; Kumar et al., 2018). Since the actual value of C_{scat} could not be determined in this study, the default value provided in the manual is used. This may lead to a systematic overestimation of the absorption coefficient. However, because C_{scat} can be regarded as a constant, the reported values at different hydrogen mole fractions remain comparable relative to each other.

A SMPS instrument developed by the Leibniz Institute for Tropospheric Research was used to measure particle size distributions. The SMPS uses a Nickel-63 source as neutralizer, followed by a differential mobility analyzer (DMA, model Vienna-DMA medium) and a condensation particle counter (CPC, model 3750 TSI). The DMA was operated using an aerosol sample flow of 1 L min^{-1} and a sheath flow of 5 L min^{-1}, resulting in a measurement range of particle mobility diameters between 8.7 and 835 nm. The raw data are inverted and corrected for multiple charges using a software package DMPS Inversion, version 2.13 (Wiedensohler et al., 2012).

In sampling position A (~65 cm above the burner), a SKC single-stage personal modular impactor with a PM2.5 cut-off at a constant flow of 4 L $min^{-1}$was used to sample the combustion particles on a quartz filter with a diameter of 37 mm. A pump is positioned after the filter sampler to provide a constant flow rate through the filter. Since some flames produced considerably more particles than other flames, various flow rates (between 1 and 4 L min^{-1}) and sampling times (between 1 minute and 5 minutes) were used in order to collect a similar mass concentration of particles on the filters, within detection limits of the OC-EC analyzer. The changes in cut-off diameter due to the changing sampling flow rate did not affect the results, as the particles produced by the flame have sizes much smaller than 2.5 µm. The temperature of the filter sampler in position A was around 80 °C.

The flow rates and sampling times were increased when operating the filter sampler in position B, since the particle concentration was significantly lower after dilution. The flow rate was increased to between 9 and 11 L min^{-1}, whereas the sampling times were ranged from 15 to 75 minutes. The sampling was tied to a tape advancement of the aethalometer: When the aethalometer changed the tape, the filter sampling was stopped immediately after.

Using a thermo-optical OC-EC analyzer (TOA model 5L, Sunset laboratory Inc.) OC, EC, and TC mass concentrations were measured following the EUSAAR2 protocol (Cavalli et al., 2010). To correct for a positive sampling artifact by adsorption of organic vapors, the filter sampler is equipped with a backup filter. The amount of OC on the backup filter is assumed to be similar to the OC mass contributed by adsorbed organic gases on the 1st filter and therefore subtracted. This was only done for filters in position B, as the carbon mass concentrations were significantly lower after dilution. Typical OC mass concentrations on the backup filter were around 0.5 µg cm^{-2}, whereas the OC mass concentration on the filter when the sampler was deployed in position A was typically more than an order of magnitude higher, up to 20 µg cm^{-2} OC. In position B, the OC

https://doi.org/10.5194/ar-2026-21
Preprint. Discussion started: 2 June 2026

AEROSOL Research Discussions

mass concentration on the filter did not exceed 5 μg cm^{-2} and was typically around 3 μg cm^{-2}. Therefore, the backup filter was deemed necessary for position B, while the correction was negligible in when operating the filter sampler in position A.

In addition, carbonaceous material from the filters in position A was dissolved in methanol and prepared for UV-vis spectroscopy, using a spectrophotometer (model USB2000, Ocean Optics) paired with a 100 cm long detection cell.

2.2 Data Analysis

The following expression is used to calculate the absorption coefficient b_{abs} from the reported by the aethalometer mass concentration of equivalent black carbon (eBC) C_{eBC} :

$$b_{\mathrm{abs}(\lambda)=C_{eBC}\cdot\sigma_{AE43}(\lambda),} \quad (4)$$

where σ_{AE43} represents the mass absorption cross sections denoted in the manual and in (Drinovec et al., 2015; Weingartner et al., 2003): 18.47, 14.54, 13.14, 11.58, 10.35, 7.77 and 7.19 m^2g^{-1}, at respectively wavelengths of 370, 420, 520, 590, 660, 880 and 950 nm.

The electrical mobility geometric mean diameter (d_g) of the particle size distribution is determined as the mode of a Gaussian fit to $\frac{dN}{dlog(d_p)}$ for every individual scan using the SMPS. For each set of flame parameters, several scans ($n \geq 3$) were conducted consecutively using the same conditions. After each batch of scans, the aerosol sampling inlet was flushed to prevent clogging, after which the procedure was repeated. The whole procedure of at least 3 scans and flushing was repeated 3 to 5 times per flame setting, resulting in at least 9 scans per flame setting. The reported geometric mean diameter (d_g) represents the average across all individual measurements, and the associated uncertainty is given as the standard deviation of those measurements.

The mass absorption cross section of the total carbonaceous aerosol is denoted by σ_{TC} and calculated as:

$$\sigma_{TC}(\lambda) = \frac{b_{abs(\lambda)}}{C_{TC}}, \quad (5)$$

where $b_{abs}(\lambda)$ is the absorption coefficient as determined by Eq. (4) and C_{TC}, is the mass concentration of total carbon in the flue gas. Only TC values from sampler position B are used to calculate the σ_{TC}, because the filter measurements at position A were conducted under a different dilution factor compared to the optical measurements.

As carbonaceous aerosol is usually subdivided into OC and EC, the light absorption properties are also reported for OC and EC separately. The mass absorption efficiency of the methanol extracted OC (denoted by σ_{dis}) is calculated as follows:

$$\sigma_{dis}(\lambda) = \frac{b_{\mathrm{abs},dis}(\lambda)}{C_{OC}}, \quad (6)$$

https://doi.org/10.5194/ar-2026-21
Preprint. Discussion started: 2 June 2026

where $b_{abs,dis}(\lambda)$ represents the absorption coefficient of the methanol-dissolved organic material at each wavelength λ and C_{OC} the mass concentration of OC defined as follows, determined by the sunset analyzer, assuming an extraction efficiency of 1, based on previous work (Ni et al., 2021). Note that therefore $b_{abs,dis}$ is normalized by OC mass, not by the total mass of organic aerosol (OA).

At the two longest wavelengths of the aethalometer (λ = 880 and 950 nm) the light absorption of OC is assumed to be negligible, and the absorption coefficient was normalized by the EC mass concentration to yield σ_{EC}:

$$\sigma_{EC(\lambda=880,950)} = \frac{b_{\mathrm{abs},(\lambda=880,950)}}{C_{EC}}, \quad (7)$$

where the b_{abs} is the absorption coefficient averaged over the sampling period (defined by the tape advance of the aethalometer) at wavelength λ = 880 and 950 nm and C_{EC} is the mass concentration of EC, determined from filter samples taken for the same flame parameters.

The absorption Ångström exponent (α) at the longest two wavelengths of the aethalometer (λ = 880 and 950 nm) is calculated as:

$$\alpha_{880-950} = \frac{-ln\left(\frac{b_{\mathrm{abs},\lambda=880}}{b_{\mathrm{abs},\lambda=950}}\right)}{ln\left(\frac{880}{950}\right)}, \quad (8)$$

The α for wavelengths between 370 nm and 660 nm (corresponding to the first 5 channels of the aethalometer) is also reported. The absorption coefficients and wavelengths of the corresponding 5 channels are plotted on a log-log scale, after which a linear regression is applied to this data. The slope of the regression line is reported as the $\alpha_{370\text{-}660}$.

2.3 1-D flame simulations

The flame temperatures as a function of flame height are determined by solving the conservation equations for 1-D flames using the Cantera package (Goodwin et al., 2017). For chemical kinetics, the San Diego mechanism (University of California, n.d.) is utilized. A mixture-averaged transport model (Kee et al., 1985) is used for calculation of transport properties. In the calculations, the computation domain is set to 6 cm. The final solution is obtained with a grid of ~120 points. A further increase in the number of grid points results in temperature changes less than 10 K. In the Cantera suite, the radiative heat losses are taken into account using the gray gas approximation in the optically thin limit (Liu and Rogg, 1991), where CO_2 and H_2O are assumed as the only radiating species. Planck mean coefficients of CO_2 and H_2O are calculated using polynomials from (Dunbar, 2006) and (Grosshandler, 1993) respectively.

The calculated flame temperature at HAB = 1 cm is chosen to represent the characteristic flame temperature. At this height, the number concentration of particles is sufficiently low (Langenkamp et al., 2018) that it justifies neglecting radiative heat

https://doi.org/10.5194/ar-2026-21
Preprint. Discussion started: 2 June 2026

losses by particles in calculations. Figure 2 shows the characteristic flame temperature as a function of hydrogen mole fraction γ at different exit velocities v_{exit}.

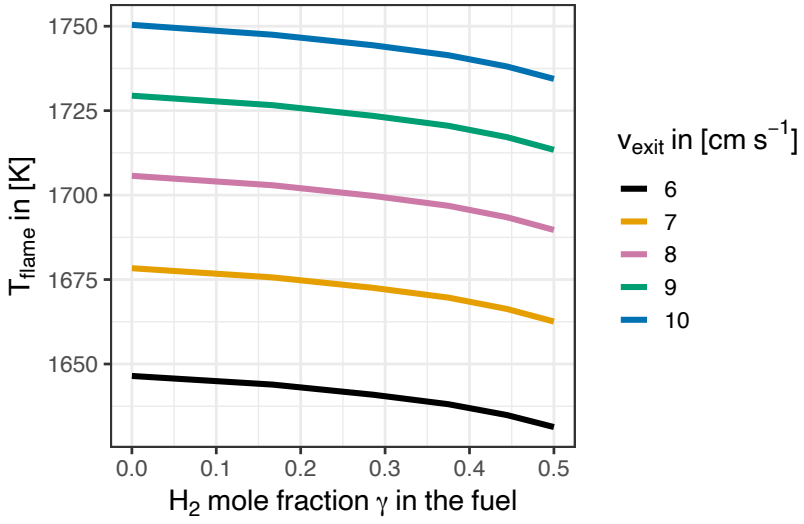

Figure 2: Calculated flame temperature at HAB of 1 cm as a function of hydrogen mole fraction and exit velocity of unburned gas mixture. Colors depict different exit velocities v_{exit}.

The characteristic flame temperatures monotonically increase between 1630 and 1750 K with increasing exit velocity from 6 to 10 cm s^{-1}. Addition of hydrogen to the fuel decreases the flame temperature because pure hydrogen flames have higher burning velocities in comparison with the burning velocities of the pure ethylene flames. However, the dependence of the flame temperature upon the exit velocity is stronger than upon the hydrogen mole fraction in the fuel.

The observed flame exhibits a conical structure, reaching a height of ~ 5 cm, indicating that 1-D flame approximation is valid only at low heights (≤ 2 cm) above the burner head. Further downstream the flames narrow and finally cease to exist due to mixing of combustion products with the surrounding shroud of nitrogen.

3 Results

3.1 Particle size and EC/TC ratios

The electrical mobility equivalent geometric mean diameter d_g is presented in Fig. 3 as a function of hydrogen mole fraction in the fuel γ, while colors depict the different exit velocities.

https://doi.org/10.5194/ar-2026-21
Preprint. Discussion started: 2 June 2026

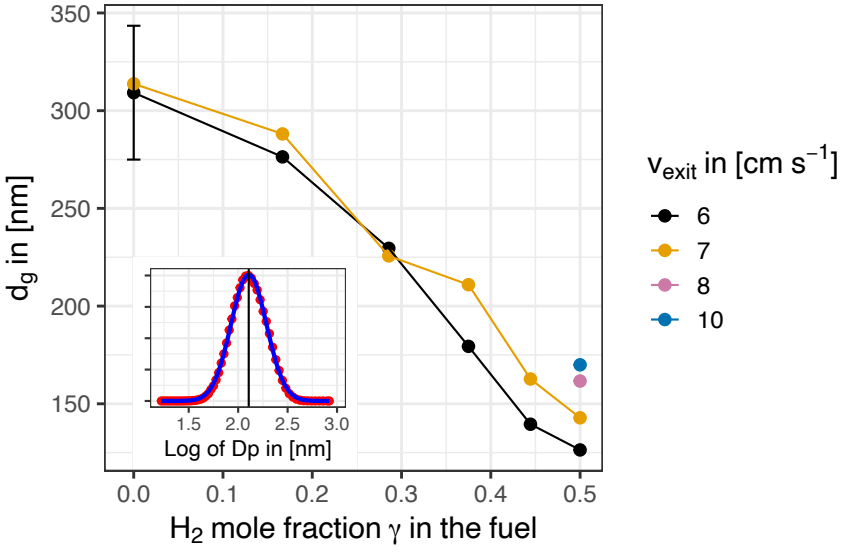

Figure 3: The effect of hydrogen addition of d_g for different exit velocities, depicted by colors. The error bar represents a typical measurement uncertainty of 10% based on repeated measurements. Lines are added to guide the eye. The particle size distribution of one arbitrary sample is shown as an insert, where the red points depict measurements and the blue line depicts the Gaussian fit on a logarithmic x-axis.

The size distribution of one arbitrary sample is shown as an inset in Fig. 3. The uncertainty of repeated measurements in d_g was typically within 10%, which is indicated with the error bar in the figure. Only two error bars are shown to improve readability. Within the measurement range of the SMPS, all flames in this study produced aerosol with a single modal size distribution. The geometric mean diameters drastically decrease with increasing hydrogen fraction, e.g. from d_g = 310 nm at γ = 0 to d_g = 125 nm at γ = 0.5. The exit velocity (and thus flame temperature and residence time) appears to have less of an impact on particle size, as d_g only marginally increases with exit velocity for γ = 0.5, while no significant change is seen for the pure ethylene flames.

EC/TC fractions of the filter samples are presented in Fig. 4, as a function of γ and v_{exit}. Measurements on replicate filters (n = 3), produced under identical flame conditions, showed variations in EC/TC within 0.07. This typical uncertainty is indicated by the error bar in the figure. For clarity, only one representative error bar is shown. Both the EC/TC fractions in position A (circular points and solid line in Fig. 4) and position B (triangular points with dashed lines in Fig. 4) are shown.

https://doi.org/10.5194/ar-2026-21
Preprint. Discussion started: 2 June 2026

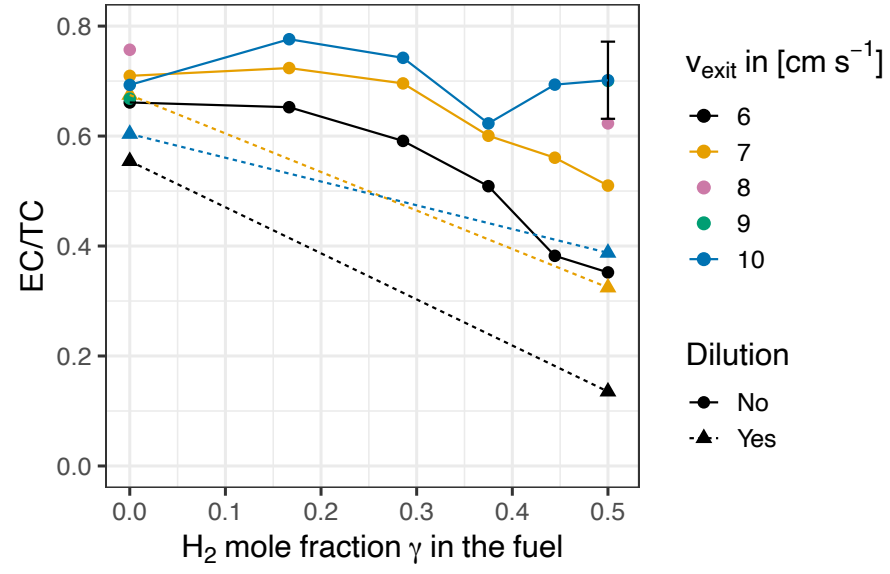

Figure 4: The effect of hydrogen addition on EC/TC ratios for different exit velocities. Both sampling positions are shown, directly above the flame and after dilution (respectively position A and B from Fig. 1). The measurement uncertainty in EC/TC of 0.07 is indicated by the error bar.

EC/TC fractions did not exceed 80%, indicating that some OC was present in the particles at all flame conditions. The pure ethylene flames produced aerosol (sampled in position A) with ~70% EC, independent of exit velocity. With larger hydrogen mole fractions in the fuel, different effects are observed: The EC/TC ratio of the flame with an exit velocity of 10 cm s^{-1} does remain around ~70%, while the colder flames (exit velocity of 6 and 7 cm s^{-1}) show a decrease of EC/TC with increasing γ. In other words, flames with high hydrogen doping combined with low exit velocities show a significant decrease in EC/TC compared to the other flames. At an exit velocity of 6 cm s^{-1} combined with a hydrogen mole fraction $\alpha = 0.5$, the EC/TC ratios decrease to below 0.5.

The EC/TC ratio decreased after extra dilution between sampling positions A and B (dashed lines). The dilution also induces cooling, where the flue gases decreased from ~80° C to room temperature. This causes gaseous organic compounds left in the exhaust to condense on the existing particles, coating the combustion-generated particles and decreasing the EC/TC fraction of the particles. However, the lower concentration of particles and gases after dilution can also cause evaporation of OC from particles, increasing the EC/TC fractions. In this case, the condensation of OC seems to exceed the evaporation of organics from the particles.

Overall, the EC/TC ratio decreases with hydrogen mole fraction in the fuel, but mostly for flames with lower temperatures (v_{exit} = 6 and 7 cm s^{-1}).

https://doi.org/10.5194/ar-2026-21
Preprint. Discussion started: 2 June 2026

AEROSOL Research Discussions

3.2 Light absorption properties of solvent-extracted OC

Filters used for solvent extraction were collected at position A from the flow directly above the flame. The σ_{dis} of solvent-extracted OC can be seen in Fig. 5 (a).

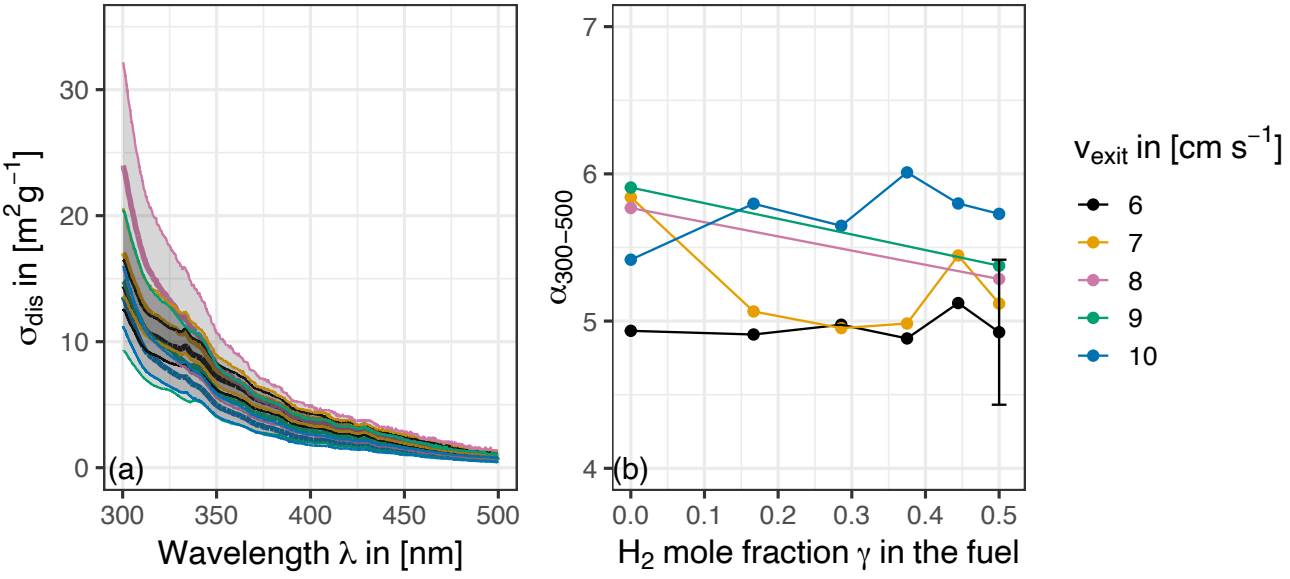

Figure 5: (a) mass absorption efficiency of methanol-dissolved OC (σ_{dis}) averaged for all hydrogen mole fractions γ and (b) the absorption Ångström exponent between 300 and 500 nm, $\alpha_{300\text{-}500}$, as a function of hydrogen mole fraction γ in the fuel. Colors depict different exit velocities, while shaded areas and error bars represent the standard deviation of several filter samples collected under the same flame conditions.

Shaded areas represent the standard deviation of several filter samples collected under the same flame conditions (n = 3). Colors represent the exit velocities. To improve readability, σ_{dis} in Fig. 5 (a) is averaged for all hydrogen mole fractions, as the change in hydrogen mole fraction did not influence the σ_{dis} significantly.

Negligible light absorption is observed at wavelengths longer than 500 nm. The σ_{dis} between 300 and 500 nm showed no clear relationship with v_{exit}. For all flame parameters, σ_{dis} increases for shorter wavelengths, reaching mass absorption efficiencies around 15 m^2g^{-1} at 300 nm. Note that the flame with intermediate flame temperature (v_{exit} = 8 m s^{-1}) produced the OC with the highest σ_{dis}. However, these results should be interpreted with caution, as they are based on only two flame conditions: γ = 0 and 0.5.

The absorption Ångström exponent between 300 and 500 nm, $\alpha_{300\text{-}500}$, is shown in Fig. 5 (b). Only one error bar representing a typical uncertainty of ± 10% is shown in Fig. 5 (b) to improve readability. $\alpha_{300\text{-}500}$ lies around 5 and 6, with no clear relationship to either the flame temperature or fuel composition. From these results, it is concluded that the optical properties of the solvent extracted OC does not change significantly for different fuel compositions and flame parameters.

https://doi.org/10.5194/ar-2026-21
Preprint. Discussion started: 2 June 2026

3.3 Particulate light absorption properties

Figure 6 shows the absorption coefficient normalized to the total carbon mass concentrations (σ_{TC}) as a function of EC/TC for three wavelengths: 370, 590 and 880 nm. Each data point corresponds to an average value of σ_{TC} based on three replicate filters. Error bars represent a typical uncertainty of 10%, based on repeated measurements from three filters produced under identical flame conditions. A dashed line following $\sigma_{TC}(\lambda) = \sigma_{TC,lit}(\lambda) \cdot \frac{EC}{TC}$ is added. This line represents the σ_{TC} of an idealized external mixture of colorless OC and EC; i.e. only EC contributes to the light absorption and its light absorption is not influenced by the presence of OC. The literature consensus value of 7.5 ± 1.2 m^2g^{-1} at 550 nm (Bond and Bergstrom, 2006) is assigned to $\sigma_{TC,lit}$, and the resulting uncertainty is indicated by the light blue shaded area. This line will be referred to as the 'external mixing line'. This implies that data points above the line exhibit stronger light absorption than the corresponding external mixture of OC and EC, potentially due to additional OC absorption at short wavelengths or due to absorption enhancement in an internal mixture of OC and EC.

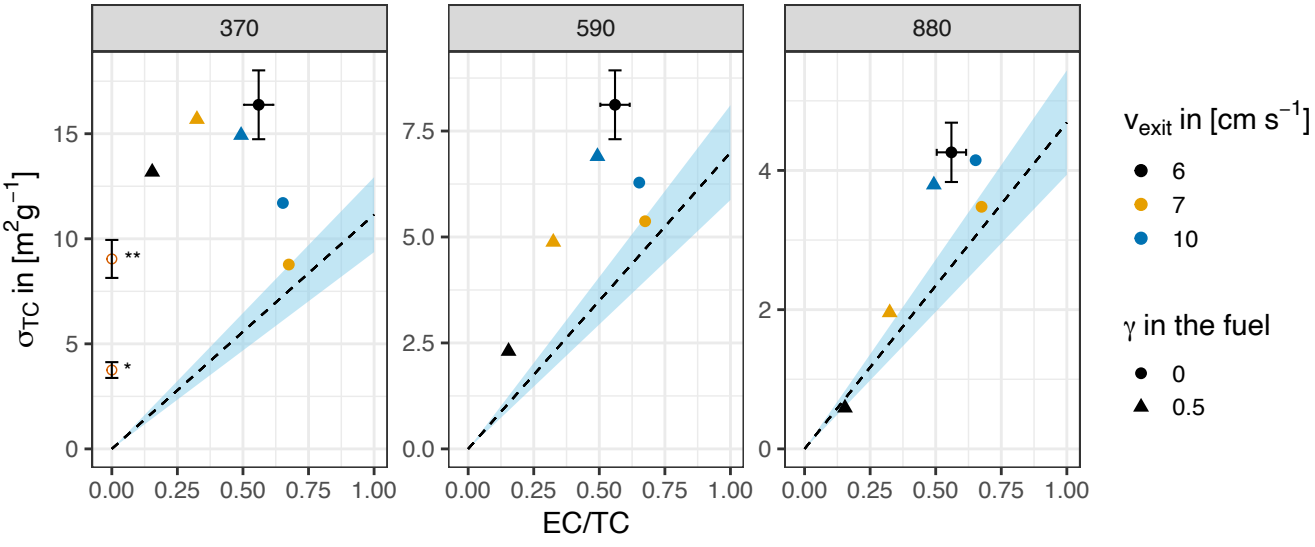

Figure 6: Mass absorption cross section σ_{TC} as a function of EC/TC fraction, at wavelengths 370 (a), 590 (b) and 880 (c) nm. The dashed line with shaded area represents σ of an idealized external mixture of colorless OC and EC (Bond and Bergstrom, 2006)**. Colors depict exit velocities, while the error bars represent the typical uncertainty of 10%, based on repeated measurements. *The estimated σ_{TC} value at EC/TC = 0 using the σ_{dis} of methanol-extracted OC, assuming Rayleigh regime** (Sun et al., 2007)**. **The estimated σ_{TC} value at EC/TC = 0 using the σ_{dis} of methanol-extracted OC, assuming Mie regime** (Liu et al., 2013).

The measured σ_{TC} values do not exhibit a linear relationship with EC/TC, indicating that a model based on externally mixed aerosols and colorless OC does not adequately describe the data. This conclusion is supported by the single modal size distributions from Fig. 3, which also points towards internal mixing, as a bimodal distribution is expected when OC and EC

https://doi.org/10.5194/ar-2026-21
Preprint. Discussion started: 2 June 2026

particles are created separately. As most points lie above the external mixing line, OC light absorption and/or internal mixing effects likely enhance σ_{TC}.

Figure 6 (c) shows σ_{TC} at 880 nm, where OC does usually not contribute to light absorption. The points are therefore close to the external mixing line, although those around EC/TC ≃ 0.5 are elevated relative to the shaded area. In fact, they are up to a factor of ~1.4 higher compared the upper bound of the external mixing line's uncertainty indicating an absorption enhancement by internally mixed OC, likely in the form of coating. The highest enhancement factors are typically observed in aged particles under atmospheric conditions, with typical values around 1.5 (Bond and Bergstrom, 2006), and reaching up to 2.4 in some modeled cases (Zhang et al., 2016).

Figure 6 (b) shows σ_{TC} at 590 nm. σ_{TC} deviates more strongly from the external mixing line than at 880 nm, as the absorption enhancement is up to ~ 1.8 compared to the upper limit of the external mixing line. This indicates the presence of colored OC absorbing light with this wavelength. From Fig. 5, the methanol-dissolved OC only marginally absorbs light at wavelengths ~ 590 nm. This indicates that if colored OC does contribute to the observed light absorption at this wavelength, it is likely not soluble in methanol. The OC-EC mixing state may also contribute to absorption enhancement at this wavelength, but likely not significantly more than at 880 nm.

Figure 6 (a) shows the σ_{TC} values at 370 nm. σ_{TC} is significantly elevated compared to the external mixing line, indicating that OC material contributes significantly to the light absorption. Especially at EC/TC fractions < 0.6, the light absorption of OC is significant and σ_{TC} does not strongly decrease towards lower EC/TC fractions, indicating comparable absorption coefficients of OC and EC at this wavelength.

Note that in general σ_{TC} values are highly dependent on the assumed C_{scat}, as discussed previously and this has consequences for comparing the present work with literature values of σ_{TC}. For example, if a C_{scat} value of 2 is assumed (a typical value in literature) the highest measured σ_{TC} would reduce from ~ 15 to ~ 11 m^2g^{-1} at 370 nm.

From Fig. 5, the methanol-dissolved OC shows significant light absorption at λ = 370 nm. To compare the σ_{dis} of methanol-dissolved OC to σ_{TC} in particulate form, a conversion factor is necessary. From Sun et al. (2007), the σ_{TC} value in small particle limit (Rayleigh regime) is found by $\sigma_{TC} = \sigma_{dis} \cdot \xi$, where ξ is called the particulate effect and depends on the refractive index of the OC material. For the real part of the refractive index m_r = 1.5 and imaginary part of the refractive index k ranging from 0.1 to 1, ξ is between 0.69 and 0.75, indicating that ξ only marginally changes with k (Sun et al., 2007).

Using ξ = 0.75, the average σ_{dis} at λ = 370 from Fig. 5 (a) converts to 3.8 m^2g^{-1}, and is indicated in Fig. 6 at EC/TC = 0 with the open orange circle, indicated by the * symbol. However, as the particle sizes can exceed 300 nm (Fig. 3), the small particle regime is not strictly applicable. Therefore, an upper limit of $\sigma_{TC} = \sigma_{dis} \cdot 1.8$ is assumed, which was previously derived for typical ambient size distributions (Liu et al., 2013). The σ_{TC} derived using this assumption is also shown in Fig. 6, indicated by the ** symbol. Since the particle size distributions in this study are smaller than those of typical ambient particles (and particles are not spherical) the σ_{TC} values derived from σ_{dis} measurements are interpreted as extremes. Specifically, values based on the small particle limit are treated as lower limits, while those from the Mie calculations cited above are considered upper limits.

https://doi.org/10.5194/ar-2026-21
Preprint. Discussion started: 2 June 2026

AEROSOL Research Discussions

Since OC does not absorb light at λ = 880 and 950 nm, the absorption coefficient can be normalized to the EC mass concentration (σ_{EC}) and compared to literature values. σ_{EC} is presented in Table 1.

370

Table 1: σ_{EC} with various v_{exit} and γ. Uncertainties depict the standard deviation of three replicate filters with the same flame parameters. For v_{exit} = 7 cm s^{-1}, only one experiment was done, although the uncertainty is expected to have similar magnitude.

v_{exit} [cm s^{-1}]	H_2 fraction γ	$\sigma_{EC,880}$ [m^2g^{-1}]	$\sigma_{EC,950}$ [m^2g^{-1}]
6	0	7.6 ± 0.3	7.0 ± 0.3
6	0.5	3.8 ± 0.2	3.1 ± 0.2
7	0	5.2	4.7
7	0.5	6.0	5.2
10	0	6.3 ± 0.2	6.0 ± 0.2
10	0.5	7.8 ± 0.6	7.1 ± 0.5

The σ_{EC} values observed in this study are generally higher than those reported in Bond and Bergstrom (2006), with values of
375 4.7 ± 0.8 m^2g^{-1} at 880 nm and 4.3 ± 0.7 m^2g^{-1} at 950 nm. However, when a hypothetical C_{scat} of 2 is applied (instead of 1.39), the values become roughly comparable. Only under the condition of γ = 0.5 and v_{exit} = 6 cm s^{-1} was σ_{EC} lower than the σ values from Bond and Bergstrom (2006). Notably, under these flame conditions, particles were produced with a very low EC/TC ratio close to 10%. At such low EC/TC fractions, it is evident that the particle maturation process is incomplete, and the EC is likely more amorphous and thus less light-absorbing than fully matured EC.

380 Comparing the different panels in Fig. 6, it shows that σ_{TC} has a clear wavelength dependence, especially at shorter wavelengths. Figure 7 (a) shows the absorption Ångström exponent ($\alpha_{370\text{-}660}$) as a function of hydrogen mole fraction γ in the fuel, and v_{exit}. Repeated experiments on different days (n ≥ 5) were typically within a range of 5%, indicated by the error bar.

https://doi.org/10.5194/ar-2026-21
Preprint. Discussion started: 2 June 2026

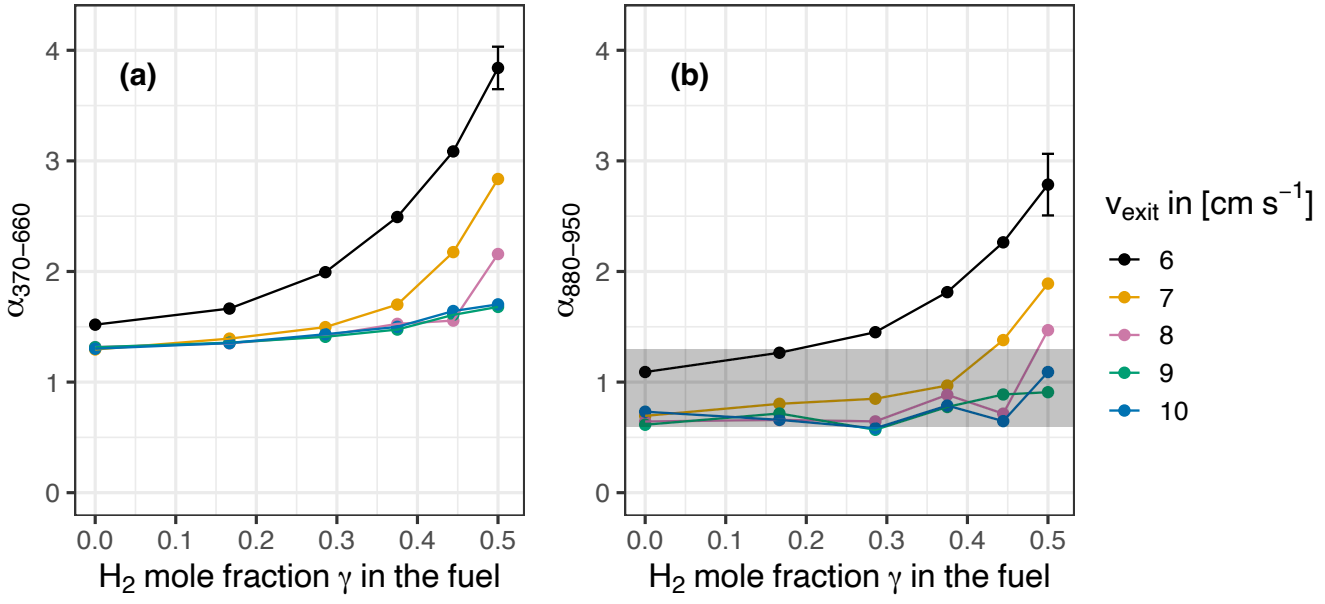

Figure 7: (a) the effect of hydrogen addition on $\alpha_{370-660}$, where colors depict different exit velocities. The error bar represents the typical measurement uncertainty of 5%. (b) the effect of hydrogen addition on $\alpha_{880-950}$, where colors depict different exit velocities. The error bar represents the typical measurement uncertainty of 10%. The gray area indicates commonly reported α values (Corbin et al., 2019; Liu et al., 2018)**.**

Each set of flames parameters produced particles with $\alpha_{370-660}$ above 1 and as high as 3.8, indicating the presence of light absorbing OC in all products. For the pure ethylene flames, $\alpha_{370-660}$ varies in a narrow range between 1.3 and 1.5, with almost no dependence on exit velocity. $\alpha_{370-660}$ increases with hydrogen mole fraction γ, especially for the lower exit velocities.

A comparison between Fig. 7 and the EC/TC results from Fig. 4 reveals an opposite trend. As γ increases, $\alpha_{370-660}$ increases while EC/TC decreases, particularly at low exit velocity. This suggests that $\alpha_{370-660}$ increases with increasing organic carbon fraction in the emitted particles.

The α with respect to the two largest wavelengths $\alpha_{880-950}$ is shown in Fig. 7 (b). Repeated measurements on different days ($n \geq 5$, where one measurement consists of a minimal 12 minutes) were typically within a range of 10%, indicated by the error bar. Absorption Ångström exponent α values between 0.8 and 1.1 are commonly reported for fresh BC (Corbin et al., 2019; Liu et al., 2018), indicated by the gray area in Fig. 8. Including the error bars, the majority of the data points were found to be within the indicated range, although some $\alpha_{880-950}$ values are slightly lower, down to 0.6. At v_{exit} = 6 cm s^{-1}, $\alpha_{880-950}$ is elevated compared to other exit velocities, reaching a value of 2.8 at γ = 0.5. Together with the low σ_{EC} observed under these conditions, this indicates that particles from these flame conditions are less mature than those formed at higher v_{exit}.

As shown in Fig. 5, the solvent-extractable OC does not exhibit significant light absorption at wavelengths shorter than 500 nm. However, $\alpha_{880-950}$ values of up to 2.8, typically associated with the presence of colored OC, are still observed at wavelengths

https://doi.org/10.5194/ar-2026-21
Preprint. Discussion started: 2 June 2026

> 880nm. These elevated α values suggest that non-extractable OC is present that contributes to light absorption at wavelengths above 800 nm. Taken together, the low σ_{EC} and the high $\alpha_{880\text{-}950}$ suggest the presence of a non-solvent extractable material with intermediate light-absorbing properties at long wavelengths: weaker than EC and with a spectral dependence larger than the typical EC value of 1.

4 Discussion

4.1 Optical properties

Both colored and colorless OC are reported as OC, although they do not have the same light absorption properties and are definitely not the same material. Following Pöschl (2005), colorless OC is expected to be low molecular weight hydrocarbons and derivatives, while some PAH-like materials can be detected as colored OC. The decreased EC/TC values after extra dilution are explained by condensing hydrocarbon gases (and derivatives) on existing particles, as the flue gases are cooled by the dilution. These gases are expected to have a relatively low molecular mass and are therefore likely colorless OC. To define the colored OC further, Corbin et al. (2019) distinguished between two types of BrC, termed tar BrC and soluble BrC. Soluble BrC typically has a σ_{dis} between 0.1 and 6.0 m^2g^{-1} at 370 nm and an $\alpha_{370\text{-}530}$ between 2 and 7. This is in line with the reported σ_{dis} and $\alpha_{300\text{-}500}$ values of solvent extracted OC presented in Fig. 5.

Saleh (2020) categorized 4 subdivisions of BrC ranging from very weakly absorptive BrC (VW-BrC) to strongly absorptive BrC (S-BrC), based on the imaginary part of the refractive index and wavelength dependence. Based on the absorption Ångström exponent reported in Fig. 5 (average $\alpha_{300\text{-}500}$ = 5.4), the methanol-extracted OC from this study lies between weakly absorptive (W-BrC) and medium absorptive (M-BrC) brown carbon regimes. Using the small-particle approximation (ξ = 0.75), the corresponding σ value at 550 nm is approximately 0.3 m^2g^{-1}, which falls within the M-BrC range (0.13–1.3 m^2g^{-1}. Since this value is close to the lower bound of the M-BrC regime, both the α and σ metrics suggest that the BrC in this study is near the transition between W-BrC and M-BrC.

The mass absorption cross section of EC values at 880 and 960 nm in this study were higher than typical literature values determined for pure BC (Bond and Bergstrom 2006). Since the particles in this study contain varying amounts of OC, both light absorption enhancement resulting from OC-EC mixing state but also a wrong assumption of C_{scat} might contribute to these elevated values of σ_{EC}. Therefore, the results from this research are compared with the σ_{EC} values from studies where EC likely has considerable coating as well. Olson et al. (2015) combusted various fuels such as pellets, diesel and lignite and reported bulk $\sigma_{EC,880}$ values up to 18 m^2g^{-1}, using a similar aethalometer. However, most of the $\sigma_{EC,880}$ values were reported between 0.2 and 5 m^2g^{-1} (Olson et al., 2015), with the lowest values found at low EC/TC ratios (EC/TC < 0.1). At slightly higher EC/TC ratios, the $\sigma_{EC,880}$ approached 5 m^2g^{-1}. Many other studies report $\sigma_{EC,880}$ values around 5 m^2g^{-1} from various sources (Cheng et al., 2019; Conrad and Johnson, 2019; J. C. Corbin et al., 2022; Kumar et al., 2018; Picca et al., 2023) and using various measurement techniques, in line with the literature consensus value of 4.7 ± 0.8 m^2g^{-1}. Although good agreement has been reported between filter-based α calculations and multi-wavelength in-situ method (Török et al., 2018), another study

https://doi.org/10.5194/ar-2026-21
Preprint. Discussion started: 2 June 2026

comparing multiple aerosol absorption instruments found consistently higher absorption coefficients (and resulting higher σ values) when using a similar aethalometer, compared to other optical measurement techniques (Kalbermatter et al., 2022). This indicates that the C_{scat} value assumed in our study is likely biased somewhat low, resulting in systematically higher σ_{EC} values. However, the nonlinear dependence of σ_{EC} on EC/TC points to a significant influence of the OC-EC mixing state on light absorption as well.

Török et al. (2018) investigated the absorption Angström exponent of particles generated using a miniCAST (with various propane and N_2 mixtures) as a function of the OC mass fraction. $\alpha_{405\text{-}1064}$ values of ~3.5 are reported for OC/TC fractions close to 0.8, similar to this research. After heating the flue gases (500 °C), $\alpha_{405\text{-}1064}$ decreased to 2.5. It is concluded that the still elevated α value after heating compared to pure BC is due to persistent OC (refractory OC) and pyrolytic carbon (PC), which is charred OC. Although the methods were not the same, similar conclusions can be drawn from this study, since an increase in $\alpha_{370\text{-}660}$ is also reported for particles with high OC mass fractions. This is shown in more detail in Fig. 8, which shows $\alpha_{370\text{-}660}$ as a function of OC/TC from this work.

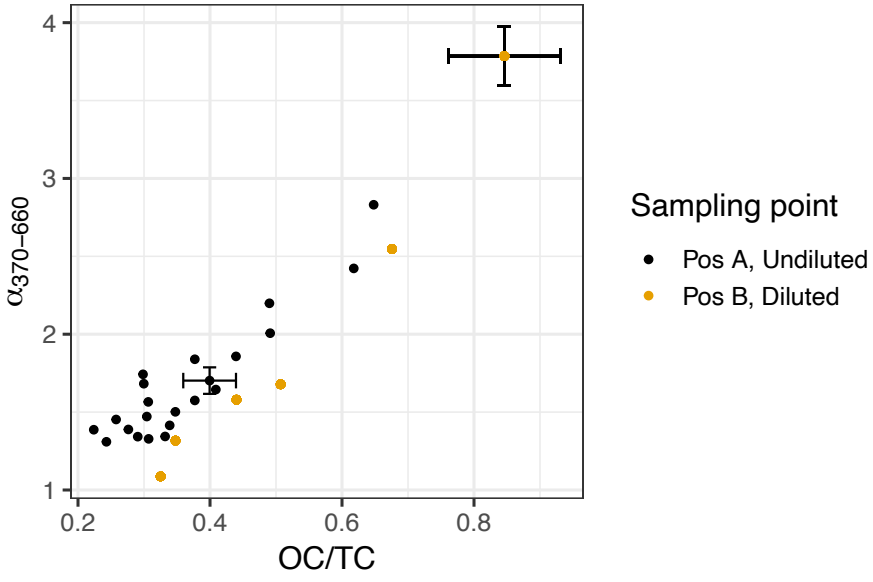

Figure 8: $\alpha_{370\text{-}660}$ as a function of OC/TC ratio. Colors represent filter sampling positions. The black points represent OC/TC ratios at the filter sampling position A, undiluted and right above the flame, while the yellow points indicate position B, where the particles are diluted and further cooled to room temperature. The $\alpha_{370\text{-}660}$ was always measured under diluted conditions. Error bars indicate the typical uncertainty found based on repeated measurements: 5% in $\alpha_{370\text{-}660}$ and 10% in OC/TC.

Note that the $\alpha_{370\text{-}660}$ values are all measured in under diluted conditions (Position B, see the experimental setup in Fig. 1), whereas the OC/TC ratios are measured using different sampling positions: In position A the particles are sampled above the flame at ~65 cm above the burner, where the flue gases are still ~80 °C, whereas in position B the sample is diluted and cooled

https://doi.org/10.5194/ar-2026-21
Preprint. Discussion started: 2 June 2026

down to room temperature. This led to a decrease in EC/TC fraction (Fig. 4), due to condensing organic compounds. As a result, the OC/TC fraction increased, causing a rightward shift of the diluted sample in Fig. 8, which is apparent despite the considerable spread in the data point particularly at low OC/TC ratios. This shift supports the interpretation that the condensing OC is colorless - or at least less light-absorbing - compared to the OC condensed at ~80 °C. Therefore, we assume that most the light absorption of OC is dominated by the OC condensed at ~80 °C, i.e. measured at sampling position A. Since the σ_{dis} of the organic material on filters collected at this position does not significantly depend on fuel composition or flame temperature (as shown in Fig. 5), the OC/TC fraction serves as a good predictor of α. Note that the particle size also systematically increases with OC/TC ratio, as can be seen by comparing Fig. 3 and Fig. 4. However, within the particle size range of our study, α is not expected to depend significantly on particle size (Malmborg et al., 2021). Therefore, it is assumed that the increasing OC fraction is the main cause of the increasing α. These observations also suggest that, under varying flame conditions, it is primarily the quantity of OC that changes, not its optical properties.

4.2 Colored OC as precursor to EC

Previous literature has found that immature combustion particles primarily consist of OC and exhibit light-absorbing properties (Malmborg et al., 2017; Maricq, 2014; Saleh et al., 2018; Török et al., 2018). As the residence time in the flame increases, these particles gradually mature, undergoing de-hybridization to form graphitic layers characteristic of EC, while also growing in size through agglomeration. Therefore, low EC/TC ratios combined with high α values and smaller particle sizes suggest incomplete maturation. In this study, increasing γ led to lower EC/TC fractions, higher α values and smaller d_g, implying that the addition of hydrogen delayed the maturation process of the combustion particles.

We suggest that the continuous progression of particle maturation mirrors a continuous increase of EC/TC ratios. However, it is possible that some materials get assigned to EC in thermos-optical analysis, although they absorb less light compared to pure BC, as also concluded in another study (Maricq, 2014). Terms such as dark BrC (d-BrC) (Chakrabarty et al., 2023) or S-BrC (Saleh, 2020) are introduced in other studies, describing particles with light absorption properties close to BC. In terms of particle maturation, this can be regarded as 'almost mature BC'. We propose that such material can be classified as EC, which results in lower σ_{EC} values compared to pure BC. This is supported by the observation that, for the flame with v_{exit} = 6 cm s^{-1} and γ = 0.5, $\sigma_{EC,880}$ was 3.8 m^2g^{-1} (lower than the consensus literature value of $\sigma_{TC,lit}$ at 4.7 m^2g^{-1}) despite likely underestimation of C_{scat}.

5 Conclusion

Combustion-generated particles from various ethylene/hydrogen mixtures were examined to find their geometric mean electrical mobility diameter (d_g), EC/TC fractions, and their light absorption properties as well as the light absorption properties of methanol-dissolved OC. Hydrogen mole fractions in the fuel ranged from 0 to 50%. A McKenna burner was used to produce premixed burner-stabilized flat flames. The exit velocity of the fuel/air mixtures ranged from 6 to 10 cm s^{-1} to produce flame

https://doi.org/10.5194/ar-2026-21
Preprint. Discussion started: 2 June 2026

temperatures ranging from 1631 to 1750 °C while keeping fuel/air ratios constant at φ = 2.3. The aerosol was sub-sampled at a height of 65 cm above the burner and subsequently diluted before analysis with an aethalometer and SMPS. The addition of hydrogen to the fuel induced a decrease of d_g from 310 nm to 125 nm. Meanwhile, a decrease of the EC/TC ratio is observed with increasing hydrogen mole fractions, although even pure ethylene flames produced aerosol containing approximately 30% OC. Especially when combining large hydrogen mole fractions with low flame temperatures, the EC/TC fraction could be as low as 15%. The smallest EC/TC fractions were reported after dilution, as gaseous organics left in the exhaust condensed on other particles after cooling, and therefore increased the OC fraction. The solvent extracted OC material showed significant light absorption at wavelengths < 500 nm. Different flame parameters and fuel composition did not significantly change the absorption coefficient normalized to methonal-soluble OC mass concentration (σ_{dis}), nor the absorption Ångström exponent at wavelengths between 300 and 500 nm ($\alpha_{300\text{-}500}$). The average σ_{dis} at 370 nm was 5.0 m^2g^{-1}. The absorption coefficient normalized to the total carbon mass (σ_{TC}) at 880 nm, was slightly elevated compared to the consensus values for pure BC, particularly at EC/TC ratios around 0.5. The σ_{EC} values, i.e. the absorption coefficient at wavelengths of 880 and 950 nm normalized to the EC mass concentration, were in the most cases also slightly elevated compared to consensus values of BC. This increase may be partly attributed to the lensing effect caused by organic coatings on the particles. The filter-based measurement technique might also contribute to this increase, by systematically overestimating the absorption coefficient of particles embedded in the filter matrix. At shorter wavelengths, the contribution of OC to the total observed light absorption increased. The absorption Angström exponent of the emitted particulate matter showed a dependence on exit velocity and hydrogen mole fraction in the fuel, increasing from 1.5 for pure ethylene to 3.8 for a hydrogen mole fraction of 0.5. The increasing $\alpha_{370\text{-}660}$ can be directly explained by increasing OC/TC ratios, at constant optical properties of the OC material. Furthermore, in line with other literature, it is proposed that part of the observed OC above the flame results from primary combustion particles that did not fully mature to EC in the presence of hydrogen. This could be due to reduced flame temperatures, but it is also possible that the presence of hydrogen otherwise impedes the de-hybridization process.

Code and data availability

The data and code to reproduce the figures are available at the Zenodo repository, DOI: 10.5281/zenodo.20340451.

Author contributions

SvR, UD, and AM designed the setup and experiments, and SvR, MvH, MG carried them out. HN did the UV-Vis measurements. SvR, UD, and AM did the data analysis. SvR composed the figures and wrote the manuscript with input from UD and AM.

https://doi.org/10.5194/ar-2026-21
Preprint. Discussion started: 2 June 2026

Competing interests

The authors declare no competing interests.

Disclaimer

Copernicus Publications remains neutral with regard to jurisdictional claims made in the text, published maps, institutional affiliations, or any other geographical representation in this paper. While Copernicus Publications makes every effort to include appropriate place names, the final responsibility lies with the authors. Views expressed in the text are those of the authors and do not necessarily reflect the views of the publisher.

Acknowledgements

The authors gratefully acknowledge the technical help of M. Bosker and J. Mulder provided during the experiments.

Financial support

This research has been supported by the Ruisdael Observatory, a scientific infrastructure co-financed by the Dutch Research Council (NWO, 184.034.015). The authors also acknowledge the project grants from the Natural Science Basic Research Program of Shaanxi (Grant No. 2024JC-YBQN-0328).

References

Andreae, M. O., and Gelencser, A.: Black carbon or brown carbon? The nature of light-absorbing carbonaceous aerosols. Atmos. Chem. Phys., 6, 3131–3148, https://doi.org/www.atmos-chem-phys.net/6/3131/2006/, 2020.

Angström, A.: On the Atmospheric Transmission of Sun Radiation and on Dust in the Air, Geografika Ann, 11, 156–166, 1929.

Bond, T. C., and Bergstrom, R. W.: Light Absorption by Carbonaceous Particles: An Investigative Review, Aerosol Science and Technology, 40:1, 27–67, https://doi.org/10.1080/02786820500421521, 2006.

Bond, T. C., Doherty, S. J., Fahey, D. W., Forster, P. M., Berntsen, T., DeAngelo, B. J., G.Flanner, M., Ghan, S., Kärcher, B., Koch, D., Kinne, S., Kondo, Y., Quinn, P. K., Sarofim, M. C., Schultz, M. G., Schulz, M., Venkataraman, C., Zhang, H., Zhang, S., Zender, C. S.: Bounding the role of black carbon in the climate system: A scientific assessment, Journal of Geophysical Research: Atmospheres, 118, 5380–5552, https://doi.org/10.1002/jgrd.50171, 2013.

https://doi.org/10.5194/ar-2026-21
Preprint. Discussion started: 2 June 2026

Cavalli, F., Viana, M., Yttri, K. E., Genberg, J., and Putaud, J.-P.: Toward a standardised thermal-optical protocol for measuring atmospheric organic and elemental carbon: the EUSAAR protocol, Atmospheric Measurement Techniques, 3, 79–89. https://doi.org/www.atmos-meas-tech.net/3/79/2010/, 2010.

Chakrabarty, R. K., Shetty, N. J., Thind, A. S., Beele, P., Sumlin, B. J., Zhang, C., Liu, P., Idrobo, J. C., Adachi, K., Wagner, N. L., Schwarz, J. P., Ahern, A., III, A. J. S., Lambe, A., Daube, C., Lyu, M., Liu, C., Herndon, S., Onasch, T. B., and Mishra, R.: Shortwave absorption by wildfire smoke dominated by dark brown carbon, Nature Geoscience, 16, 683–688. https://doi.org/10.1038/s41561-023-01237-9, 2023.

Cheng, Z., Atwi, K., Onyima, T., and Saleh, R., Investigating the dependence of light-absorption properties of combustion carbonaceous aerosols on combustion conditions, Aerosol Science and Technology, 53, 419–434. https://doi.org/https://doi.org/10.1080/02786826.2019.1566593, 2019.

Conrad, B. M., and Johnson, M. R.: Mass absorption cross-section of flare-generated black carbon: Variability, predictive model, and implications, Carbon, 149, 760–771, https://doi.org/10.1016/j.carbon.2019.04.086, 2019.

Corbin, J. C., Czech, H., Massabò, D., de Mongeot, F. B., Jakobi, G., Liu, F., Lobo, P., Mennucci, C., Mensah, A. A., Orasche, J., Pieber, S. M., Prévôt, A. S. H., Stengel, B., Tay, L.-L., Zanatta, M., Zimmermann, R., Haddad, I. El, and Gysel, M.: Infrared-absorbing carbonaceous tar can dominate light absorption by marine-engine exhaust, Npj Clim Atmos Sci, 2, 2–12, https://doi.org/10.1038/s41612-019-0069-5, 2019.

Corbin, J. C., Johnson, T. J., Liu, F., Sipkens, T. A., Johnson, M. P., Lobo, P., and Smallwood, G. J.: Size-dependent mass absorption cross-section of soot particles from various sources, Carbon, 192, 438–451, https://doi.org/10.1016/j.carbon.2022.02.037, 2022.

Corbin, J. C., Pieber, S. M., Czech, H., Zanatta, M., Jakobi, G., Massabò, D., Orasche, J., Haddad, I. El, Mensah, A. A., Stengel, B., Drinovec, L., Mocnik, G., Zimmermann, R., Prévôt, A. S. H., and Gysel, M.: Brown and Black Carbon Emitted by a Marine Engine Operatedon Heavy Fuel Oil and Distillate Fuels: Optical Properties, Size Distributions, and Emission Factors, Journal of Geophysical Research: Atmospheres, 123(11), 6175–6195, https://doi.org/10.1029/2017JD027818, 2018.

Corbin, J., Modini, R., and Gysel-Beer, Ma., Mechanisms of soot-aggregate restructuring and compaction, Aerosol Science and Technology, 57(2), 89–111, https://doi.org/10.1080/02786826.2022.2137385, 2023.

Drinovec, L., Mocnik, G., Zotter, P., Prévôt, A. S. H., Ruckstuhl, C., Coz, E., Rupakheti, M., Sciare, J., Müller, T., Wiedensohler, A., and Hansen, A. D. A.: The dual-spot Aethalometer: an improved measurement of aerosol black carbon with real-time loading compensation, Atmos. Meas. Tech., 8, 1965–1979, https://doi.org/10.5194/amt-8-1965-2015, 2015.

Dunbar, W. R.: Planck Mean Absorption Coefficients of H_2O, CO_2, CO, and NO for Radiation Modeling in Combustion, Journal of Quantitative Spectroscopy and Radiative Transfer, 97(1), 20–38, 2006.

Ferrero, L., Losi, N., Rigler, M., Gregoric, A., Colombi, C., D'Angelo, L., Cuccia, E., Cefali, A. M., Gini, I., Doldi, A., Cerri, S., Maroni, P., Cipriano, D., Markuszewski, P., and Bolzacchini, E.: Determining the Aethalometer multiple scattering enhancement factor C from the filter loading parameter, Science of the Total Environment, 917, 170221, https://doi.org/10.1016/j.scitotenv.2024.170221, 2024.

https://doi.org/10.5194/ar-2026-21
Preprint. Discussion started: 2 June 2026

García, A., Verdugo, I., Cruz, J. J., Escudero, F., Yap, V., Gallardo, J., Demarco, R., Yon, J., and Fuentes, A., Effect of hydrogen addition on soot maturity and volume fraction of ethylene non-premixed flames under different oxygen indices, Proceedings of the Combustion Institute, 40(1), 105539, https://doi.org/https://doi.org/10.1016/j.proci.2024.105539, 2024.

Goodwin, D. G., Moffat, H. K., and Speth, R. L.: Cantera: An Object-oriented Software Toolkit for Chemical Kinetics, Thermodynamics, and Transport Processes, Zenodo, https://doi.org/10.5281/zenodo.170284, 2017.

Grosshandler, W. L.: RADCAL: A Narrow-Band Model for Radiation Calculations in a Combustion Environment (Issue NIST Technical Note 1402), https://www.nist.gov/publications/radcal-narrow-band-model-radiation, 1993.

Gülder, Ö. L., Snelling, D. R., and Sawchuk, R. A.: Influence of hydrogen addition to fuel on temperature field and soot formation in diffusion flames, Symposium (International) on Combustion, 26(2), 2351–2358, https://doi.org/10.1016/S0082-0784(96)80064-6, 1996.

Hui, X., Zheng, D., Tan, W., Xue, X., and Liu, W.: The effects of hydrogen addition on soot formation in counterflow diffusion n-heptane flames, International Journal of Hydrogen Energy, 48(23), 8707–8715, https://doi.org/10.1016/j.ijhydene.2022.12.016, 2023.

IPCC: Anthropogenic and Natural Radiative Forcing. Climate Change 2013: The Physical Science Basis, Contribution of Working Group I to the Fifth Assessment Report of the Intergovernmental Panel on Climate Change, 2023.

Jin, H., Guo, J., Li, T., Zhou, Z., Im, H. G., and Farooq, A.: Experimental and numerical study of polycyclic aromatic hydrocarbon formation in ethylene laminar co-flow diffusion flames, Fuel, 289, 119931, https://doi.org/https://doi.org/10.1016/j.fuel.2020.119931, 2021.

Kalbermatter, D. M., Mocnik, G., Drinovec, L., Visser, B., Röhrbein, J., Oscity, M., Weingartner, E., Hyvärinen, A.-P., and Vasilatou, K.: Comparing black-carbon- and aerosol-absorption-measuring instruments – a new system using lab-generated soot coated with controlled amounts of secondary organic matter, Atmospheric Measurement Techniques, 15, 561–572, https://doi.org/10.5194/amt-15-561-2022, 2022.

Kee, R. J., Miller, J. A., Smooke, G. D., and Miller, J. A.: PREMIX: A Fortran Program for Modeling Steady Laminar One-Dimensional Premixed Flames (Issues SAND85-8240), https://doi.org/10.2172/5416213, 1985.

Khanehzar, A., Cepeda, F., and Dworkin, S. B.: The influence of nitrogen and hydrogen addition/dilution on soot formation in coflow ethylene/air diffusion flames, Fuel, 309, 122244, https://doi.org/https://doi.org/10.1016/j.fuel.2021.122244, 2022.

Kumar, N. K., Corbin, J. C., Bruns, E. A., Massabó, D., Slowik, J. G., Drinovec, L., Mocnik, G. M., Prati, P., Vlachou, A., Baltensperger, U., Gysel, M., El-Haddad, I., and Prévôt, A. S. H.: Production of particulate brown carbon during atmospheric aging of residential wood-burning emissions, Atmos. Chem. Phys., 18, 17843–17861, https://doi.org/10.5194/acp-18-17843-2018, 2018.

Lack, D. A., and Langridge, J. M.: On the attribution of black and brown carbon light absorption using the Ångström exponent, Atmos. Chem. Phys, 13, 10535–10543, https://doi.org/10.5194/acp-13-10535-2013, 2013.

https://doi.org/10.5194/ar-2026-21
Preprint. Discussion started: 2 June 2026

Langenkamp, P. N., van Oijen, J. A., Levinsky, H. B., and Mokhov, A. V.: Growth of Soot Volume Fraction and Aggregate Size in 1D Premixed C2H4/Air Flames Studied by Laser-Induced Incandescence and Angle-Dependent Light Scattering, Journal of Combustion, v2018, 1–13, https://doi.org/10.1155/2018/2308419, 2018.

Liu, C., Chung, C. E., Yin, Y., and Schnaiter, M.: The absorption Ångström exponent of black carbon: from numerical aspects, Atmos. Chem. Phys., 18, 6259–6273, https://doi.org/https://doi.org/10.5194/acp-18-6259-2018, 2018.

Liu, F., and Rogg, B.: Modelling of thermally radiating diffusion flames with detailed chemistry and transport, Combustion Science and Technology, 75(1–3), 81–98, https://doi.org/10.1080/00102209108951704, 1991.

Liu, F., Yon, J., Fuentes, A., Lobo, P., Smallwood, G. J., and Corbin, J. C., Review of recent literature on the light absorption properties of black carbon: Refractive index, mass absorption cross section, and absorption function, Aerosol Science and Technology, 54:1, 33–51, https://doi.org/10.1080/02786826.2019.1676878, 2019.

Liu, J., Bergin, M., Guo, H., King, L., Kotra, N., Edgerton, E., and Weber, R. J.: Size-resolved measurements of brown carbon in water and methanol extracts and estimates of their contribution to ambient fine-particle light absorption, Atmos. Chem. Phys., 13, 12389–12404, https://doi.org/10.5194/acp-13-12389-2013, 2013.

Liu, Y., Cheng, X., Li, Y., Qiu, L., Wang, X., and Xu, Y.: Effects of ammonia addition on soot formation in ethylene laminar diffusion flames, Fuel, 292, 120416, https://doi.org/10.1016/j.fuel.2021.120416, 2021.

Malmborg, V. B., Eriksson, A. C., Shen, M., Nilsson, P., Gallo, Y., Waldheim, B., Martinsson, J., Andersson, O., and Pagels, J.: Evolution of In-Cylinder Diesel Engine Soot and Emission Characteristics Investigated with Online Aerosol Mass Spectrometry, Environmental Science and Technology, 51, 1876–1885, https://doi.org/10.1021/acs.est.6b03391, 2017.

Malmborg, V., Erikssona, A., Gren, L., Török, S., Shamun, S., Novakovic, M., Zhang, Y., Kook, S., Tuner, M., Bengtsson, P.-E., and Pagels, J.: Characteristics of BrC and BC emissions from controlled diffusion flame and diesel engine combustion, Aerosol Science and Technology, 55, 769–784, https://doi.org/10.1080/02786826.2021.1896674, 2021.

Maricq, M. M.:Examining the Relationship Between Black Carbon and Soot in Flames and Engine Exhaust, Aerosol Science and Technology, 48, 620–629, https://doi.org/10.1080/02786826.2014.904961, 2014.

Martins, J. V., Artaxo, P., Liousse, C., Reid, J. S., Hobbs, P. V, and Kaufman, Y. J.: Effects of black carbon content, particle size, and mixing on light absorption by aerosols from biomass burning in Brazil, Journal of Geophysical Research, 103, 32041–32050, 1998.

Montgomery, M. J., Kwon, H., Dreyer, J. A. H., Xuan, Y., McEnally, C. S., and Pfefferle, L. D.: Effect of ammonia addition on suppressing soot formation in methane co-flow diffusion flames, Proc. Combustion Institute, 38, 2497–2505, https://doi.org/10.1016/j.proci.2020.06.094, 2021.

Myhre, G., Samset, B. H., Schulz, M., Balkanski, Y., Bauer, S., Berntsen, T. K., Bian, H., Bellouin, N., Chin, M., Diehl, T., Easter, R. C., Feichter, J., Ghan, S. J., Hauglustaine, D., Iversen, T., Kinne, S., Kirkevag, A., Lamarque, J.-F., Lin, G., Zhou, C.: Radiative forcing of the direct aerosol effect from AeroCom Phase II simulations, Atmos. Chem. Phys, 13, 1853–1877, 2013.

https://doi.org/10.5194/ar-2026-21
Preprint. Discussion started: 2 June 2026

Ni, H., Huang, R.-J., Pieber, S. M., Corbin, J. C., Stefenelli, G., Pospisilova, V., Klein, F., Gysel-Beer, M., Yang, L., Baltensperger, U., Haddad, I. El, Slowik, J. G., Cao, J., Prévot, A. S. H., and Dusek, U.: Brown Carbon in Primary and Aged Coal Combustion Emission, Environment Science and Technology, 55, 5701–5710, https://doi.org/https://doi.org/10.1021/acs.est.0c08084, 2021.

Olson, M. R., Garcia, M. V., Robinson, M. A., Rooy, P. Van, Dietenberger, M. A., Bergin, M., and Schauer, J. J., Investigation of black and brown carbon multiple-wavelength dependent light absorption from biomass and fossil fuel combustion source emissions, Journal of Geophysical Research: Atmospheres, 120, 6682–6697, https://doi.org/10.1002/2014JD022970, 2015.

Picca, F., Sasso, F., Commodo, M., and Minutolo, P.: A Filter-Based Approach for the Measurement of MassAbsorption Coefficient of OC and EC Components in Soot, Combustion Science and Technology, 195, 3529–3541, https://doi.org/10.1080/00102202.2023.2239465, 2023.

Pöschl, U.: Atmospheric Aerosols: Composition, Transformation, Climate and Health Effects, Atmospheric Chemistry, 44, 7520–7540, https://doi.org/10.1002/anie.200501122, 2005.

Ren, F., Cheng, X., Gao, Z., Huang, Z., and Zhu, L.: Effects of NH3 addition on polycyclic aromatic hydrocarbon and soot formation in C2H4 co-flow diffusion flames, Combustion and Flame, 241, 111958, https://doi.org/10.1016/j.combustflame.2021.111958, 2022.

Saleh, R.: From Measurements to Models: Toward Accurate Representation of Brown Carbon in Climate Calculations, Current Pollution Reports, 6, 90–104, https://doi.org/https://doi.org/10.1007/s40726-020-00139-3, 2020.

Saleh, R., Cheng, Z., and Atwi, K.: The Brown−Black Continuum of Light Absorbing Combustion Aerosols, Environmental Science and Technology Letters, 5, 508–513, https://doi.org/10.1021/acs.estlett.8b00305, 2018.

Senser, D. W., Morse, J. S., and Cundy, V. A.: Construction and novel application of a flat flame burner facility to study hazardous waste combustion, Review of Scientific Instruments, 56, 1279–1284, https://doi.org/10.1063/1.1137992, 1985.

Sun, H., Biedermann, L., and Bond, T. C.: Color of brown carbon: A model for ultraviolet and visible light absorption by organic carbon aerosol, Geophysical Research Letters, 34, L17813, https://doi.org/10.1029/2007GL029797, 2007.

Török, S., Malmborg, V. B., Simonsson, J., Eriksson, A., Martinsson, J., Mannazhi, M., Pagels, J., and Bengtsson, P.-E.: Investigation of the absorption Ångström exponent and its relation to physicochemical properties for mini-CAST soot, Aerosol Science and Technology, 52, 757–767, https://doi.org/10.1080/02786826.2018.1457767, 2018.

University of California. (n.d.). Chemical-Kinetic Mechanisms for Combustion Applications, San Diego Mechanism web page, Mechanical and Aerospace Engineering, University of California at San Diego, https://web.eng.ucsd.edu/mae/groups/combustion/mechanism.html.

Warnatz, J., Maas, U., and Dibble, R. W.: Combustion (4th ed.), Springer 2006.

Weingartner, E., Saatho, H., Schnaiter, M., Streit, N., Bitnar, B., and Baltensperger, U.: Absorption of light by soot particles: determination of the absorption coefficient by means of aethalometers, Aerosol Science, 34, 1445–1463, 2003.

Wiedensohler, A., Birmili, W., Nowak, A., Sonntag, A., Weinhold, K., Merkel, M., Wehner, B., Tuch, T., Pfeifer, S., Fiebig, M., Fjäraa, A. M., Asmi, E., Sellegri, K., Depuy, R., Venzac, H., Villani, P., Laj, P., Aalto, P., Ogren, J. A., Bastian, S.:

https://doi.org/10.5194/ar-2026-21
Preprint. Discussion started: 2 June 2026

Mobility particle size spectrometers: harmonization of technical standards and data structure to facilitate high quality long-term observations of atmospheric particle number size distributions. Atmospheric Measurement Techniques, 5, 657–685. https://doi.org/10.5194/amt-5-657-2012, 2012.

Wu, R., Song, X., He, T., Gong, Y., Luo, Q., Jing, Y., Wang, J., Bai, Y., and Yu, G.: Study on the microstructure and soot formation mechanism of hydrogen addition ethylene inverse diffusion flame, International Journal of Hydrogen Energy, 88, 39–51, https://doi.org/https://doi.org/10.1016/j.ijhydene.2024.09.092, 2024.

Xi, J., Yang, G., Cai, J., and Gu, Z.: A Review of Recent Research Results on Soot: The Formation of a Kind of Carbon-Based Material in Flames, Frontiers in Materials, 8, 695485, https://doi.org/10.3389/fmats.2021.695485, 2021.

Yan, F., Xu, L., Wang, Y., Park, S., Sarathy, S. M., and Chung, S. H.: On the opposing effects of methanol and ethanol addition on PAH and soot formation in ethylene counterflow diffusion flames, Combustion and Flame, 202, 228–242, https://doi.org/10.1016/j.combustflame.2019.01.020, 2019.

Yus-Díez, J., Bernardoni, V., Mocnik, G., Alastuey, A., Ciniglia, D., Ivancic, M., Querol, X., Perez, N., Reche, C., Rigler, M., Vecchi, R., Valentini, S., and Pandolf, M.: Determination of the multiple-scattering correction factor and its cross-sensitivity to scattering and wavelength dependence for different AE33 Aethalometer filter tapes: a multi-instrumental approach, Atmos. Meas. Tech., 14, 6335–6355, https://doi.org/10.5194/amt-14-6335-2021, 2021.

Zhang, Y., Zhang, Q., Cheng, Y., Su, H., Kecorius, S., Wang, Z., Wu, Z., Hu, M., Zhu, T., Wiedensohler, A., and He, K.: Measuring the morphology and density of internally mixed black carbon with P2 and VTDMA: new insight into the absorption enhancement of black carbon in the atmosphere, Atmospheric Measurement Techniques, 9, 1833–1846, https://doi.org/10.5194/amt-9-1833-2016, 2016.

Zhao, W., Tan, W., Zhao, G., Shen, C., Yu, Y., and Zhao, C.: Determination of equivalent black carbon mass concentration from aerosol light absorption using variable mass absorption cross section, Aerosol Measurements Techniques, 14, 1319–1331, https://doi.org/https://doi.org/10.5194/amt-14-1319-2021, 2021.